Detailed materials and methods

Mouse models and allograft studies

Tyr-rtTA (1); Cdkn2a (Ink4a/Arf$^{-/-}$); Pten$^{L/L}$ (2); *Tyr-CreERT2* (3) (IP) mice in mixed FVB/C57Bl/6 strain were crossed with *tetO-PTPN11^{E76K}* mice (4) to generate tet-inducible PTPN11^{E76K} bitransgenic (BT) mice and intercrossed for 4 generations to minimize strain background effect. A tumor cohort was topically treated with 4-OHT (10 mM) on postnatal P3, P4, and P5 days and was fed with doxycycline (200 mg/kg) chow at weaning. Mice were observed for development of tumors or appearance of ill health. Premoribund animals or animals with significant tumor burdens were sacrificed, and detailed autopsies were performed. Tumor specimens were fixed in 10% formalin and embedded in paraffin for histological analysis, as previously described (5). For the allograft studies, on the indicated days post-implantation, mice were euthanatized, and tumors were excised for weight measurement and analysis.

Plasmids, shRNAs, siRNAs, inhibitors, and antibodies

The PTPN11 G503V mutation was made by PCR. cDNA encoding PTPN11 wt, E76K (4), CSDA (6), or G503V mutant was cloned into a lentiviral expression vector (pLenti-P) that carried a puromycin-resistant gene similar to that described (7). pTripZ-shRNA against PTPN11 (TAGCGTATAGTCATGAGCG) was obtained from Dharmacon. pCDNA3-HA-GSK3β-wt (Addgene #14753) and -K85A mutant (#14755) were a gift from Dr. Woodgett, mutagenized to generate Y216A via site-directed mutagenesis, and cloned into pLEX304 (# 25890, from Dr. David Root). siRNAs targeting human PTPN11 (A: SASI_Hs01_00207375, B: SASI_Hs01_00207376) and mouse Ptpn11 (C: SASI_Mm02_00304544, D: SASI_Mm02_00304545) were obtained from Sigma-Aldrich. Pharmacological inhibitors, SHP099 (6-(4-amino-4-methylpiperidin-1-yl)-3-(2,3-dichlorophenyl) pyrazine-2-amine hydrochloride) (8) were from MedChem Express, MEK162 from LC laboratories, and CHIR-99021 from Selleck chemicals. Primary antibodies were purchased from Cell Signaling Technology (pERK, ERK, PTPN11, pPTPN11 (Y542), pGab1(Y627, 659), pGSK3α/β (Ser21/9), pTyr (p-Tyr-1000)), Thermo Scientific (pGSK3α/β (Y279/216)), Invitrogen (pHIPK1/HIPK2/HIPK3 (Tyr352/361/359), pDYRK2/4 (Tyr386/268)), and Sigma-Aldrich (β-actin, FLAG).

Cell culture, in vitro assays, immunoblotting, and immunohistochemistry

Human melanoma cell lines (WM1366, WM1361A, WM1346, 1205Lu, IGR1, 983C, WM3211, MeWO, and CHL1, obtained from Dr. Meenhard Herlyn and Lynda Chin) as well as mouse melanoma cell lines (5037, 2187, W331, PA662T, and PA624T) were cultured in RPMI-1640 media containing 10% fetal bovine serum and 1% penicillin and streptomycin at 37 degrees Celsius with 5% CO_2. 5037 and 2187 cells (derived from *NRAS Q61K; Ink4a/Arf-/-)* were gifts from Dr. Lynda Chin and Lawrence Kwong, and PA662T and PA624T were derived from IP mice and W331 from BT mice in this study. Short tandem repeat (STR) and sequencing analysis for mutations in *NRAS* and *BRAF* have been performed and used within 5 passages for Human melanoma cell lines. Active Ras-GTP levels were determined using Ras Activation Assay Kits (Millipore), following the manufacturer's instructions. Western blotting, immunohistochemistry, and soft agar-colony formation assays were performed as described in our previous study (9). For cell survival assays, cells were seeded in a 96-well plate in triplicate, treated with SHP099

(0-30 μM, PTPN11 inhibitor) with or without CHIR-99021 (1 or 3 μM, GSK3α/β inhibitor) for 72hrs and fixed with 10% formalin followed by Crystal Violet staining. Statistical analysis was done using two-tailed *t-tests*. Each experiment was repeated at least two times in triplicate and representative results from one experiment are shown.

Supplementary Figure S1.

A. Schematic of whole exome sequencing performed on melanomas (PA662T, PA543T, and PA624T) tumors arising from IP mice along with matched normal tissues (A). This analysis identified 140 somatic single nucleotide variants (SNVs) and small indels. Among them, 16 nonsynonymous SNVs and 1 frame shift mutation caused coding changes in 16 genes (Supplementary table 1). Olfactory receptor (Olfr) gene variants were discarded, since Olfr have much higher mutation rates than background due to their strikingly late replication timing (10). The final list consists of 13 SNVs in 12 genes, which include several orthologous mutations observed in human tumors (Fig. 1D). **B.** Table demonstrating per sample target coverage statistics for whole exome sequence analysis. **C.** Mutation spectrum of the base changes from three tumors analyzed by whole exome sequencing. Compared to human, mouse melanoma genomes harbor much lower number of mutations and do not show the C-to-T transitions characteristic of the UV signature.

Supplemental Figure S2. Mutation and Structure analysis of PTPN11

PTPN11 mutations identified in human melanoma in multiple cancer studies (**A**). Alignment of PTPN11 sequence around S502 position among different species (**B**). Crystal structure of PTPN11 (PDB: SHP2). Blue: N-SH2 domain, Gray: C-SH2 domain, Green: PTP domain. Interaction between E76-S502 and G59-Q510 in the N-SH2 domain and PTP domain are highlighted (**C**).

Supplemental Figure S3.

Immunohistochemical staining of human melanoma tissues (formalin-fixed paraffin embedded) with pPTPN11 (Y542) antibody utilizing Vulcan Red chromogen (pink). Note the staining in the melanin positive melanoma cells.

Supplemental Figure S4.

Number of colonies grown in soft agar (Top, seeded in triplicate) by PA662T (mouse melanoma cells from *Cdkn2a(Ink4a/Arf)* $^{L/L}$*; Pten*$^{L/L}$*; Tyr-CreER*^{T2} mice) with vector control, E76K, or S502P mutant *PTPN11* (bottom: western blot) is shown graphically as mean +/- SD (*p*-value: two-tailed T-test).

Supplemental Figure S5. Signaling analysis of PA662T cell lines with overexpression of wt of activated mutant PTPN11 (**A-C**) and PA624T and 5037 (NRAS Q61K mutant) cells with Ptpn11 KD via siRNAs (C and D) or with siNT (non-targeting) control (**D**). Total cell lysates (tcl) or active Ras-GTP (pull down with RAF binding domain) were analyzed by western blot with indicated antibodies.

Supplemental Figure S6. Effects of PTPN11 knockdown in *BRAF* and *NRAS* wild type human melanoma cell lines. PTPN11 knockdown following treatment with 2ug/mL doxycycline in cells expressing doxycycline-inducible pTripZ-shPTPN11 construct significantly decreased growth in soft agar in WM3211 (p=0.011; two-tailed t-test) (**A top**) and MeWo (P=0.0497; two-tailed t-test) (**B top**) cells. PTPN11 knockdown and ERK phosphorylation were confirmed by Western analysis (**A & B bottom**).

Supplemental Figure S7. PTPN11 E76K expression drives melanoma formation and is required for tumor maintenance in genetically engineered mouse model.

Kaplan-Meier melanoma free survival curve shows decreased survival of BT (PTPN11 E76K positive) compared to MT of IP mice (p=0.0157, log-rank test). Only BT mice on doxycycline developed melanoma (**A**). Melanoma developed in a BT mouse regressed following doxycyline withdrawal, which escaped doxycyline regulation over the time course (**B**).

Supplemental Figure S8.

Representative IHC stained images of W331 subcutaneous tumors at D0, D4 and D7 after doxycycline withdrawal. Stained for Flag, pERK, pH3, and Cleaved Caspase-3 (**A**). Western analysis of W331 subcutaneous tumors harvested on D0, D3 or D7 after doxycycline withdrawal (de-induction of PTPN11 E76K) (**B**).

Supplemental Figure S9.

Heat map of pTyr-containing peptides decreased by PTPN11 E76K in both PA662T and W331 tumors (**A**). Levels of selected pTyr proteins detected in each run with tumors of PA662T with control, wt, or E76K PTPN11, and tumors of W331 D0 (on Doxy; PTPN11 E76K On) and D3 (3 day post doxy withdrawal; PTPN11 E76K Off) (**B**). **C&D**: Tables of pTyr-containing peptides regulated by PTPN11 E76K both in PA662T and W331. Delta (Δ) is a difference in median peptide abundances between E76K + vs. E76K -samples for W331 and 662T cells. P-values were calculated from LC-MS/MS data analysis by LIMMA algorithm. Peptides with $p \leq 0.05$ (**C**) and ones with highest fold change (Δ) (**D**) were shown. Western analysis of total cell lysates used in co-immunoprecipitation of PA662T cells with vector control or CSDA mutant PTPN11 in Figure 5F (**E**).

Supplemental Figure S10. Fold changes in tumor volume compared to D0 were shown over the course of treatment for individual subcutaneous tumors generated with 5037 *NRAS* mutant melanoma cells. Mice were treated with vehicle (black line) or SHP099 (100mg/kg, p.o. q.d.) (**A**). Note responders (red) with tumor regression and partial responders (blue) with suppressed growth. IHC staining for pERK, Ki67 (proliferation), and cleaved caspase-3 (apoptosis) of tumors treated with vehicle or SHP099 (at 2hrs post last dose) for the indicated number of days (**B**).

Supplemental Figure S11. Response to PTPN11 inhibition requires GSK3α/β activation Western analysis showing the expression of phosphotyrosine deficient (Y216A) or kinase dead (K85A) GSK3β in 5037 and W331 mouse melanoma cells (**A**). The number of colonies grown in soft agar by W331 cells with vector, Y216A-GSK3β, or K85A-GSK3β +/-Dox (mean +/- SD) (**B**). The effect of SHP099 in 5037 cells with vector, Y216A-GSK3β, or K85A-GSK3β on pERK, ERK, p-β-catenin, cyclin D1, and β-actin was assessed by Western analysis (**C**). Western analysis of the GSK3α/β inhibitor (CHIR-99021, 0, 3, or 10 μM) on response of pGSK3α/β (S21/9 and Y279/216) and p-β-catenin to SHP099 (30uM) (**D**).

Supplemental Figure S12. Differential response of 5037 allograft tumors to MEK162 (MEK inhibitor) vs. SHP099. Fold change in tumor volume of 5037 allograft tumors (as mean ratio to D0 +/- SEM) following treatment with vehicle, MEK162 (MEK inhibitor), or SHP099 (SHP2 inhibitor) (n=2 per group) (**A**). Note tumor stasis with MEK inhibition as previously reported mice (11), while SHP099 decreased tumor volume. IHC for pERK after 3 days of treatment with vehicle, MEK162, or SHP099 (**B**). Western analysis of pPTPN11, pERK, pGSK3α/β (S21/9 and Y279/216) along with GSK3α/β effectors including β-catenin and cyclin D1 (**C**).

Supplemental Figure S13. Effect of combining PTPN11 inhibition with MEK inhibition (trametinib) in melanoma cell lines. Western analysis showing the effect of combining trametinib (0, 1, or 10 nM) with SHP099 (30 μM) on pERK (**A**). Cell survival curves of *NRAS* mutant WM1366 melanoma cells treated with increasing concentrations of trametinib (1- 100 nM range) with or without SHP099 (30uM). Cell were seeded in triplicate and treated for 72 hrs. Data is shown as mean relative survival (compared to DMSO or SHP099 alone control) +/- SD (**B)**. WM1366 cells were grown as spheroids and then implanted into collagen with vehicle, trametinib (10 nM), SHP099 (30 μM) or trametinib (10 nM) combined with SHP099 (30 μM) for 24 hrs prior to staining with propidium iodide (PI) to show dead cells (**C**).

Supplemental Figure S14. Model of PTPN11 signaling axis in melanoma. PTPN11 functions as an oncogene in melanoma in part by activating RAS-MEK-ERK along with the Gab1-PI3K-AKT pathway and by inhibiting GSK3α/β resulting in increased Cyclin D1 and β-catenin. The resulting effect is increased proliferation, decreased apoptosis, and decreased senescence in PTPN11 activated melanomas.

Supplementary References

1. Bardeesy N, *et al.* (2005) Role of epidermal growth factor receptor signaling in RAS-driven melanoma. *Mol Cell Biol* 25(10):4176-4188.
2. Zheng H, *et al.* (2008) p53 and Pten control neural and glioma stem/progenitor cell renewal and differentiation. *Nature* 455(7216):1129-1133.
3. Bosenberg M, *et al.* (2006) Characterization of melanocyte-specific inducible Cre recombinase transgenic mice. *Genesis* 44(5):262-267.
4. Schneeberger VE, *et al.* (2014) SHP2E76K mutant promotes lung tumorigenesis in transgenic mice. *Carcinogenesis* 35(8):1717-1725.
5. Nogueira C, *et al.* (2010) Cooperative interactions of PTEN deficiency and RAS activation in melanoma metastasis. *Oncogene* 29(47):6222-6232.
6. Schneeberger VE, *et al.* (2015) Inhibition of Shp2 suppresses mutant EGFR-induced lung tumors in transgenic mouse model of lung adenocarcinoma. *Oncotarget* 6(8):6191-6202.
7. Sun X, *et al.* (2018) Selective inhibition of leukemia-associated SHP2(E69K) mutant by the allosteric SHP2 inhibitor SHP099. *Leukemia* 32(5):1246-1249.
8. Chen YN, *et al.* (2016) Allosteric inhibition of SHP2 phosphatase inhibits cancers driven by receptor tyrosine kinases. *Nature* 535(7610):148-152.
9. Sung H, *et al.* (2016) Inactivation of RASA1 promotes melanoma tumorigenesis via R-Ras activation. *Oncotarget* 7(17):23885-23896.
10. Lawrence MS, *et al.* (2013) Mutational heterogeneity in cancer and the search for new cancer-associated genes. *Nature* 499(7457):214-218.
11. Kwong LN, *et al.* (2012) Oncogenic NRAS signaling differentially regulates survival and proliferation in melanoma. *Nat Med* 18(10):1503-1510.

A

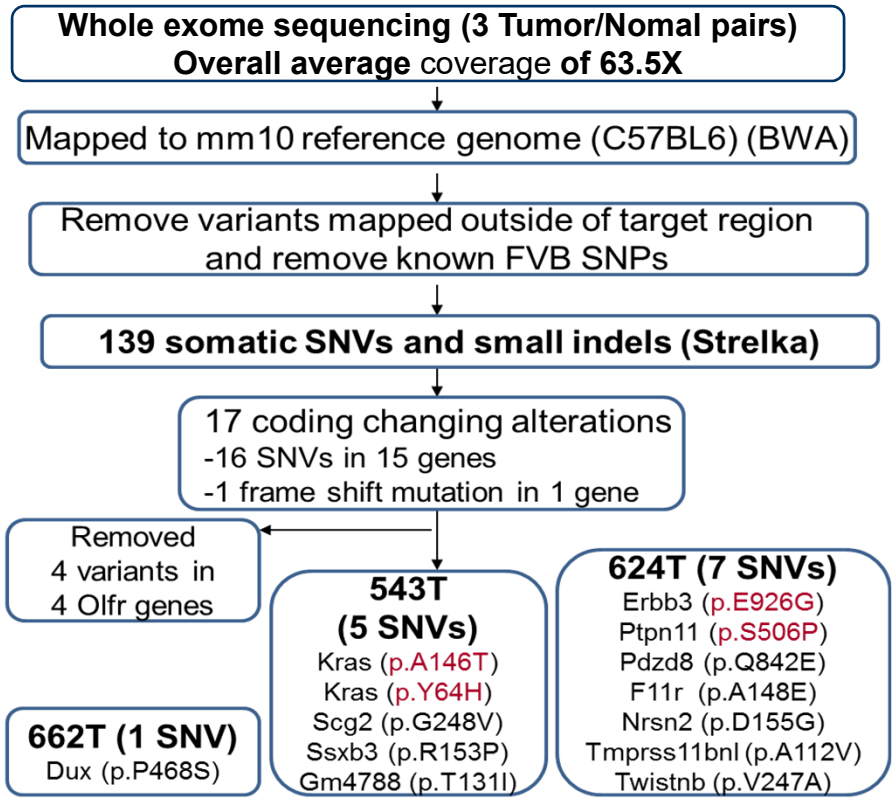

C

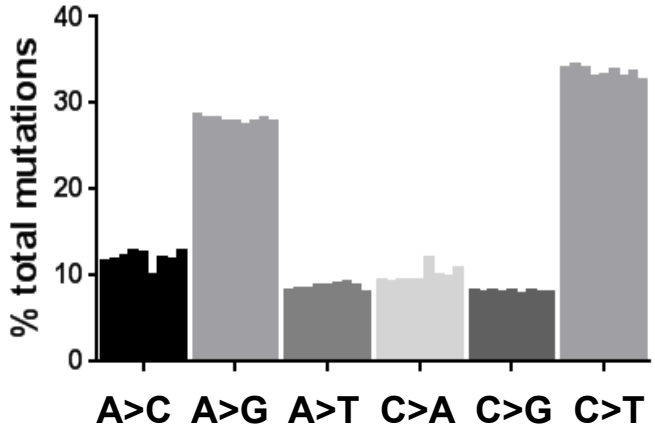

B

	library	read pairs	avg. cov.	median cov.	>5X	>10X	picard dupl,	Samtools dupl.	FastQC dupl.	avg. w/o dupl.	median w/o dupl.	needed [avg.]	needed [avg. w/o dupl.]
543T	IL4853	100,200,400	64.9X	43.8X	97.10%	94.50%	12%	10.60%	29.40%	57.1X	38.6X	0	0
543N	IL4854	84,642,473	62.2X	39.9X	97.30%	94.20%	17.60%	16.10%	37.40%	51.2X	32.9X	0	0
624T	IL4855	80,679,495	64.8X	43.6X	97.60%	95.10%	16.20%	15.10%	33.20%	54.3X	36.5X	0	0
624N	IL4856	80,398,341	81.5X	45.6X	97.70%	95.40%	15.60%	14.70%	33.40%	68.8X	38.5X	0	0
662T	IL4857	68,165,760	60.2X	39.9X	97.50%	94.20%	13.30%	12.10%	32.20%	52.2X	34.6X	0	0
662N	IL4859	49,317,128	51.1X	19.8X	89.70%	76.20%	26.80%	25.50%	50.80%	37.4X	14.5X	0	9,987,002

Supplementary Fig.S1

A

Cancer Study	Mutation rate	Sample ID	Protein_Change	Mutation_Type
Melanoma (Broad)	1.7% (2/121)	ME002	MUTATED	splice_region
		MEL-JWCI-WGS-32	Y375D	Missense
Melanoma (TCC)	2.4% (5/209)	101232837	G464A	Missense
		DS-49834	P107S	Missense
		DS-50338	I309V	Missense
			P491L	Missense
		DS-54276	S44F	Missense
		DS-80522	P561L	Missense
Melanoma (TCGA)	2.4% (7/287)	TCGA-D3-A5GS-06	P33L	Missense
		TCGA-EE-A180-06	G407Wfs*39	Frame_Shift_Ins
			T468M	Missense
		TCGA-EE-A181-06	F71L	Missense
		TCGA-EE-A2GR-06	L262F	Missense
			T468M	Missense
		TCGA-EE-A2M5-06	C563F	Missense
		TCGA-EE-A2MD-06	H114Y	Missense
		TCGA-ER-A19P-06	G60R	Missense
Melanoma (Yale)	2.2% (2/91)	YUDAB	Q506P	Missense
		YUKLAB	D425N	Missense
			P491L	Missense
			Q510L	Missense

C

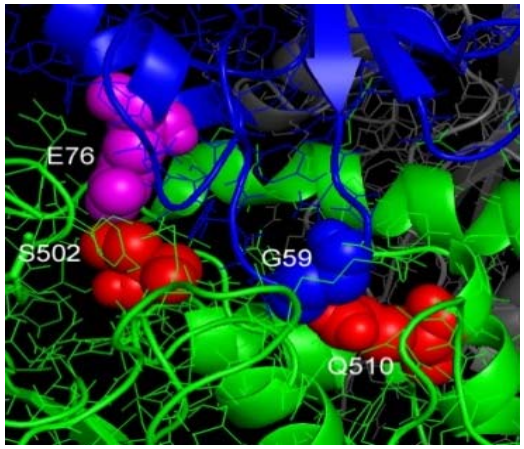

B

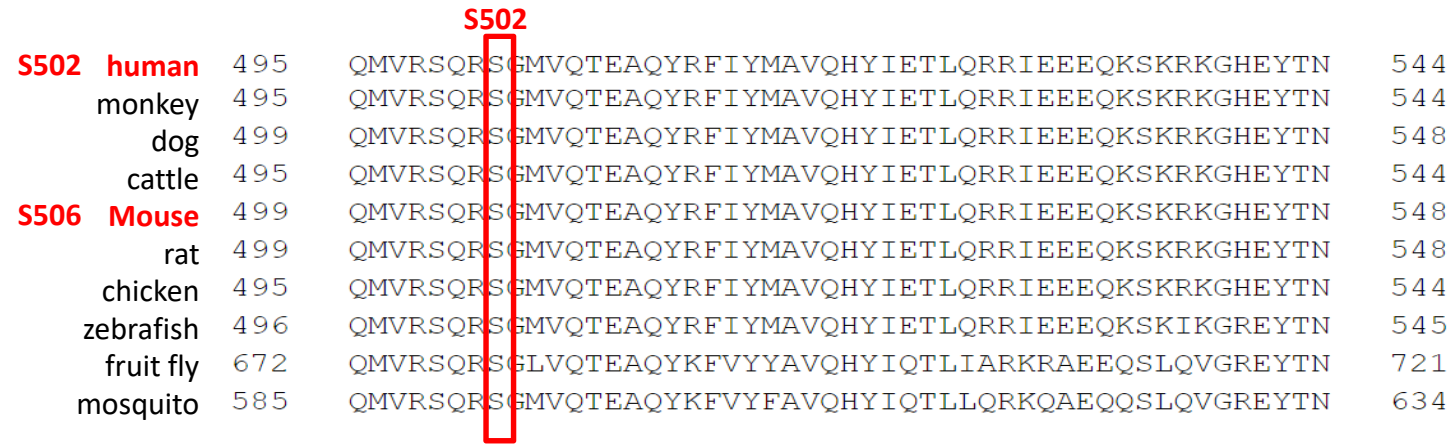

Supplementary Fig.S2

A

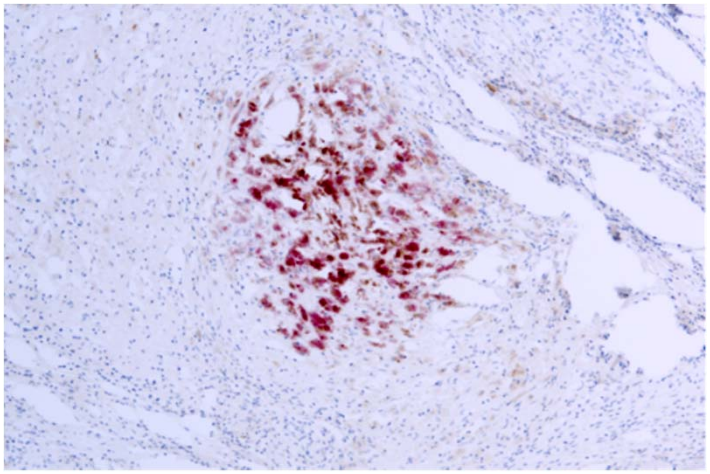

BRAF V600E
post treatment with
Dabrafenib (BRAF)/Trametinib (MEK)

B

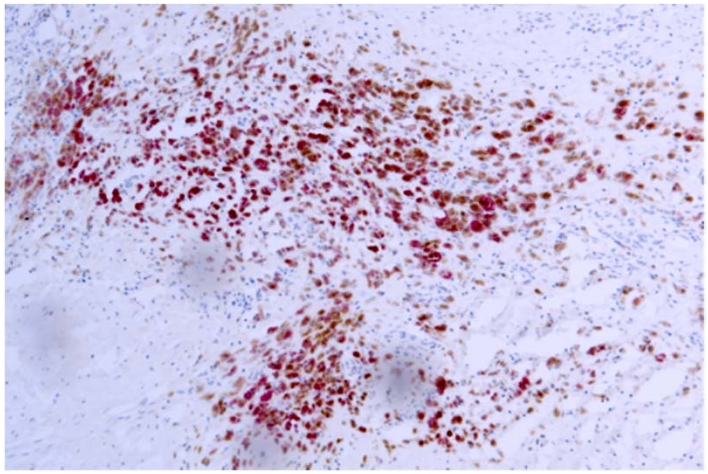

NRAS Q61R
Progressed on Trametinib treatment

Supplementary Fig.S3

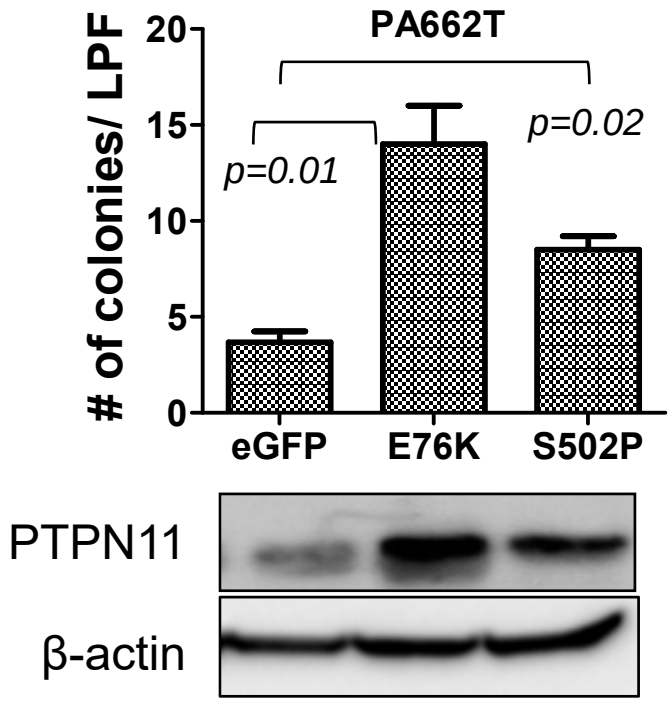

Supplementary Fig.S4

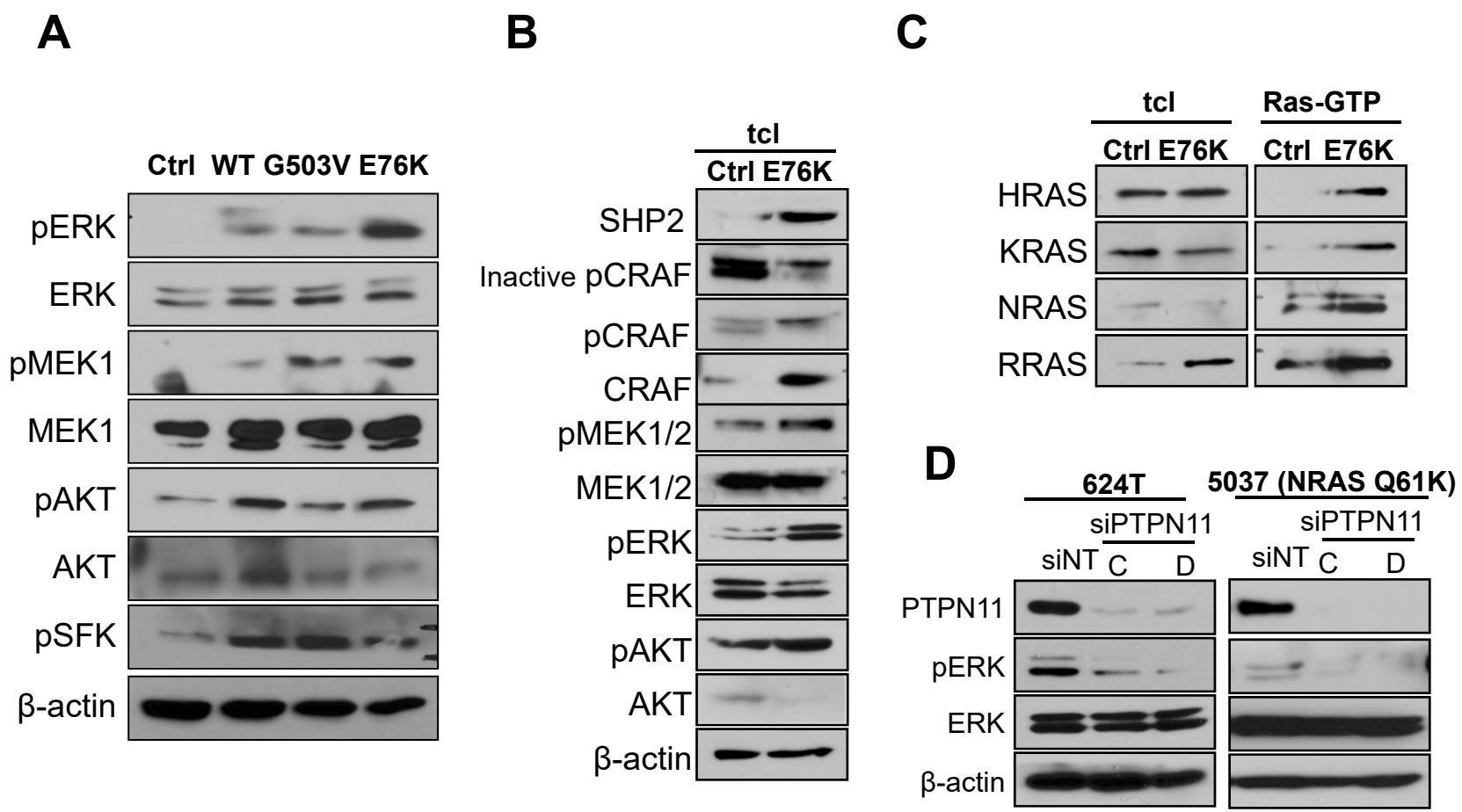

Supplementary Fig. S5

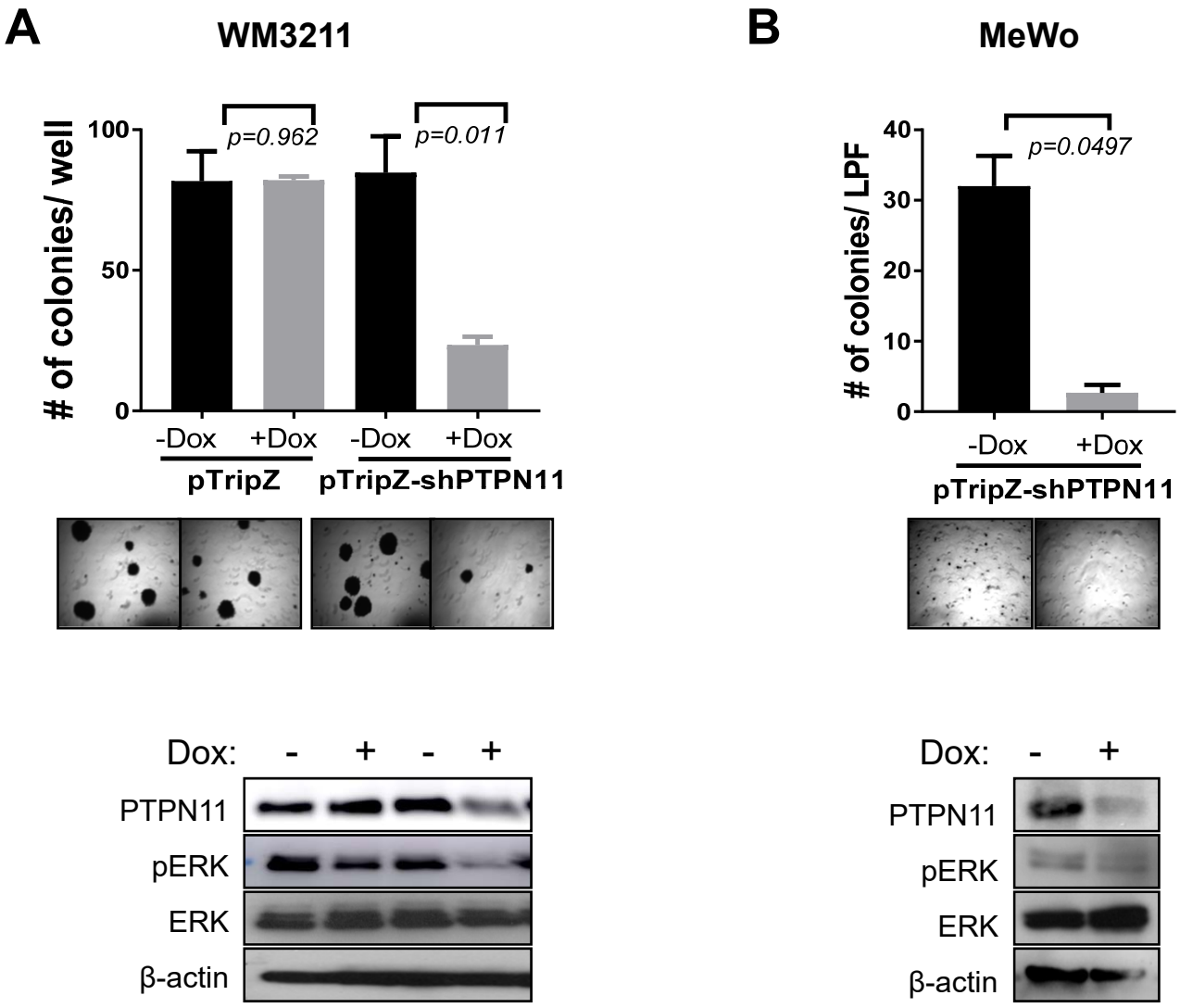

Supplementary Fig. S6

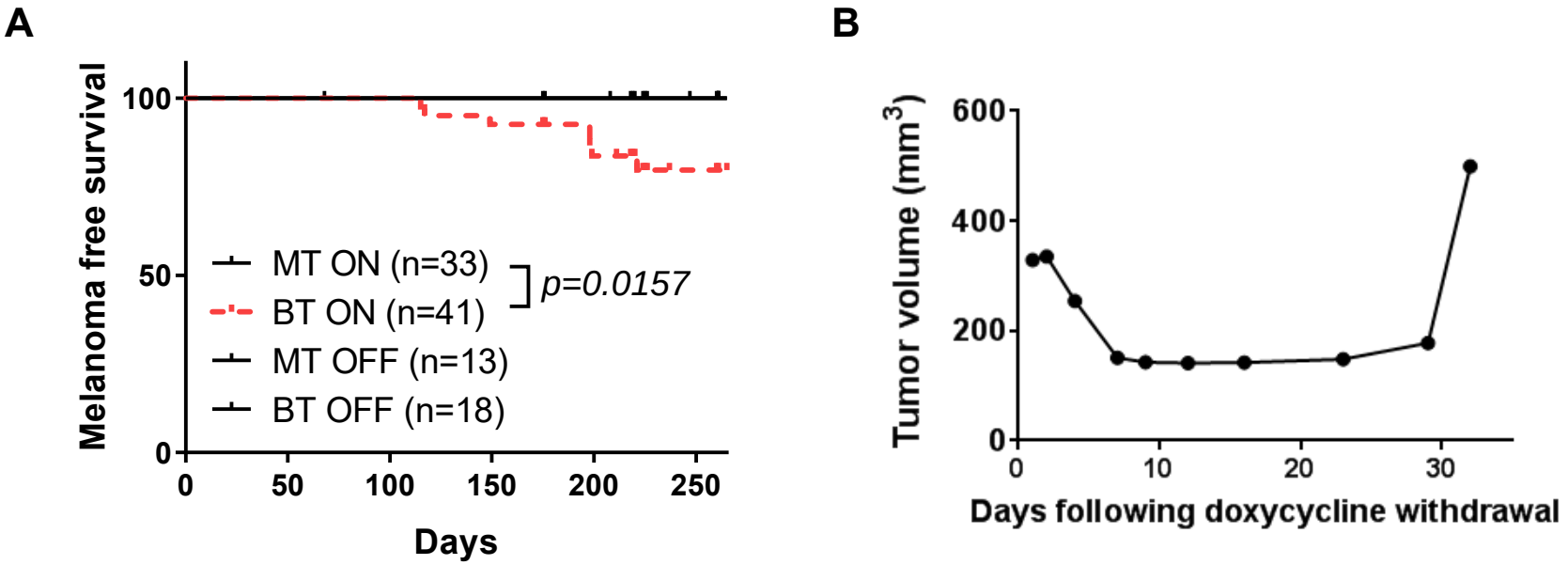

Supplementary Fig. S7

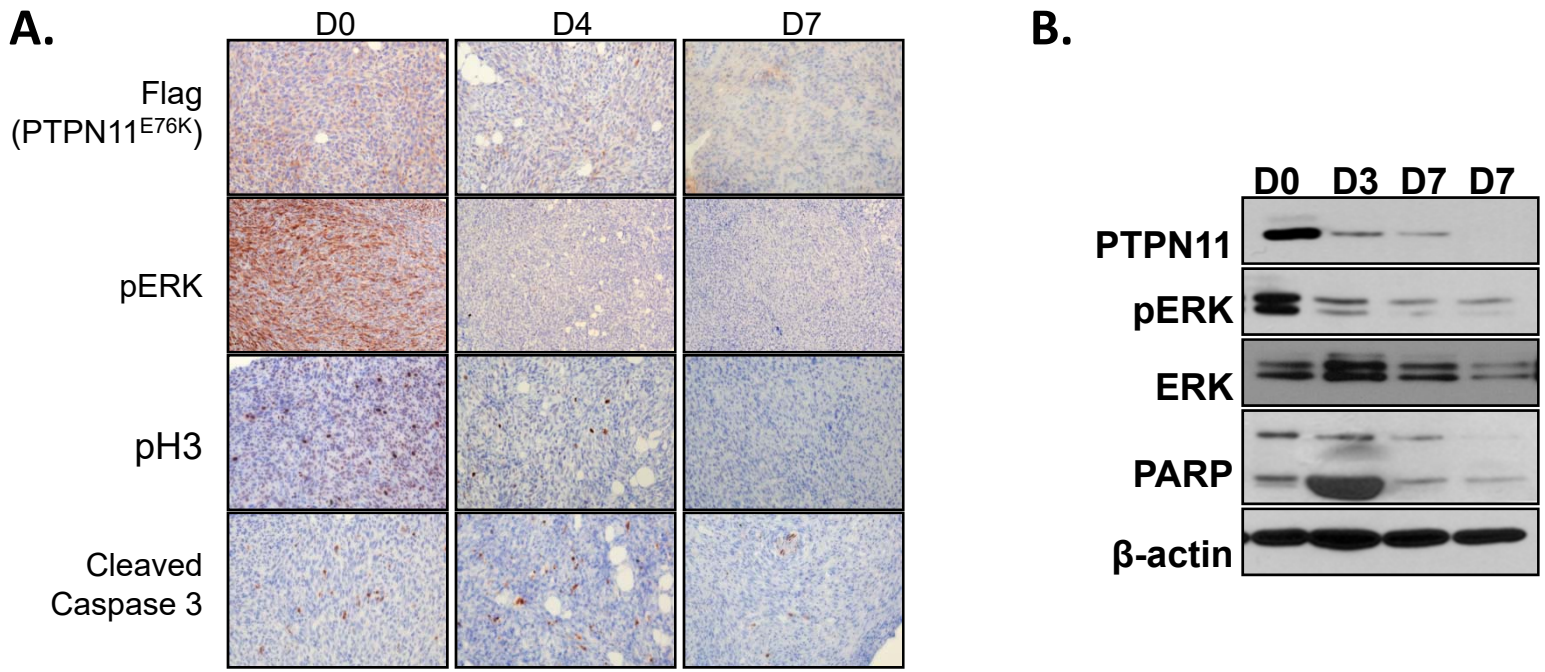

Supplementary Fig. S8

A.

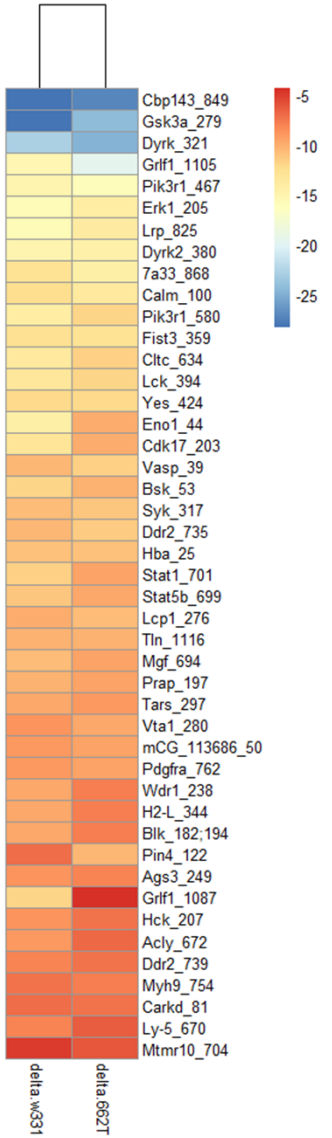

B.

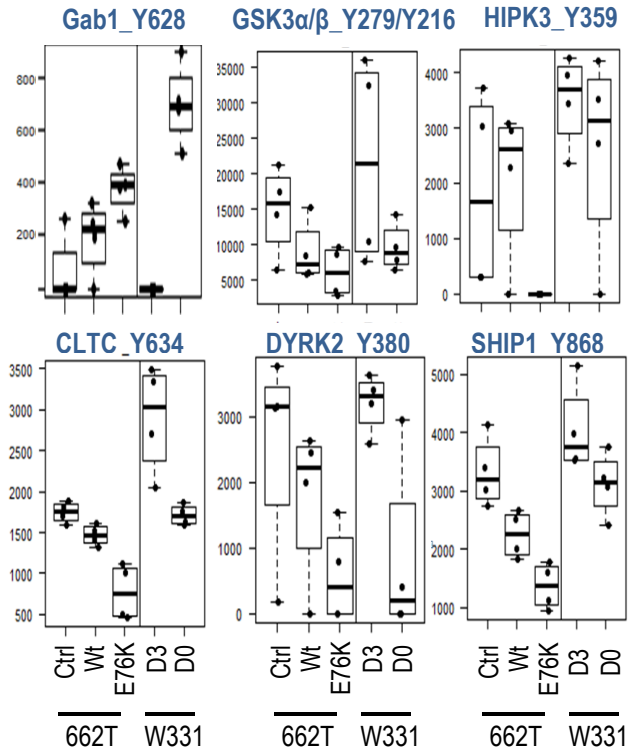

C.

UniProt ID	Name	Tyr position	W331		PA662T	
			FDR	Δ	FDR	Δ
O55033	Nck2	50	0.012	-5.71E+05	0.002	-7.24E+05
Q68FD5	Cltc	634	0.051	-6.38E+06	0.001	-2.46E+06
P06800	Ptprc	670	0.015	-2.67E+05	0.002	-6.53E+04
Q9QYY0	Gab1	628	0.020	4.78E+05	0.017	1.52E+05
Q5U4C9 Q8BI55	Dyrk2 Dyrk4	380	0.023	-1.08E+07	0.079	-9.57E+06
Q3UND0	Prap	197	0.033	-1.08E+06	0.078	-7.69E+05

D.

UniProt ID	Name	Tyr position	W331		PA662T	
			FDR	Δ	FDR	Δ
Q61136	Prpf4	849	0.184	-5.11E+08	0.010	-4.03E+08
Q2NL51 Q9WV60	Gsk3a Gsk3b	279	0.195	-5.03E+08	0.097	-2.11E+08
Q61214 Q9Z188	Dyrk1a Dyrk1b	321	0.228	-1.42E+08	0.000	-2.29E+08
Q91YM2	Grlf1	1105	0.282	-1.31E+07	0.069	-5.73E+07
P26450 Q64143	Pik3r1 Pik3r3	467	0.160	-1.15E+07	0.003	-1.70E+07
Q5U4C9 Q8BI55	Dyrk2 Dyrk4	380	0.023	-1.08E+07	0.079	-9.57E+06

E.

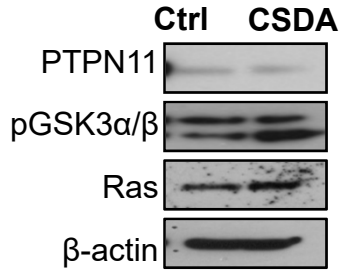

Supplementary Fig. S9:

A.

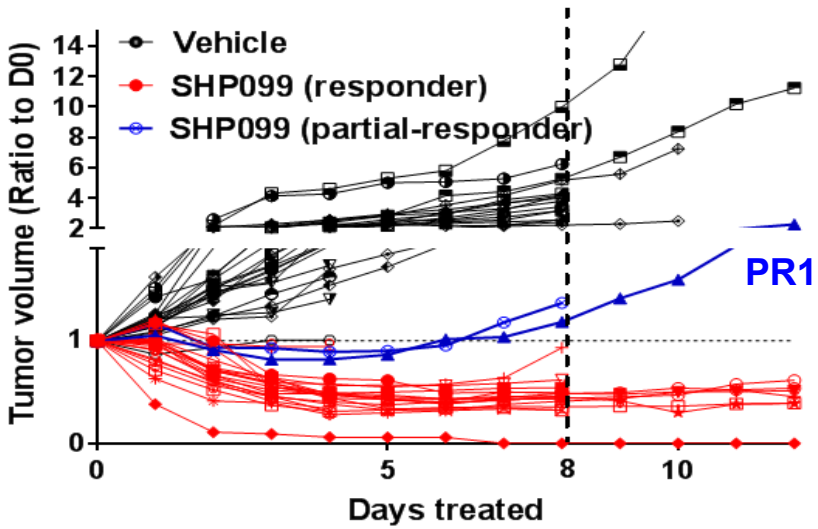

B.

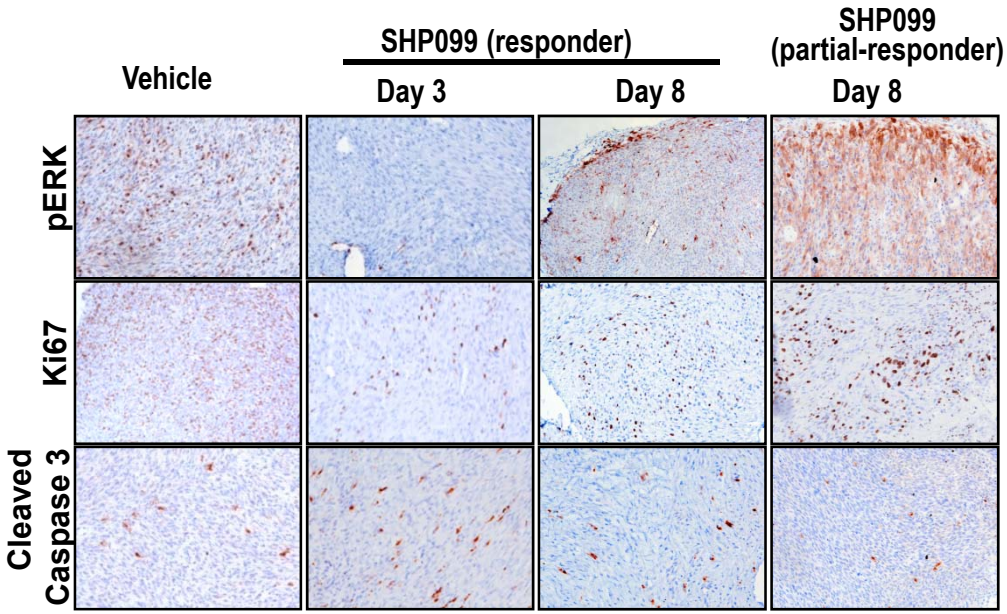

Supplementary Fig. S10

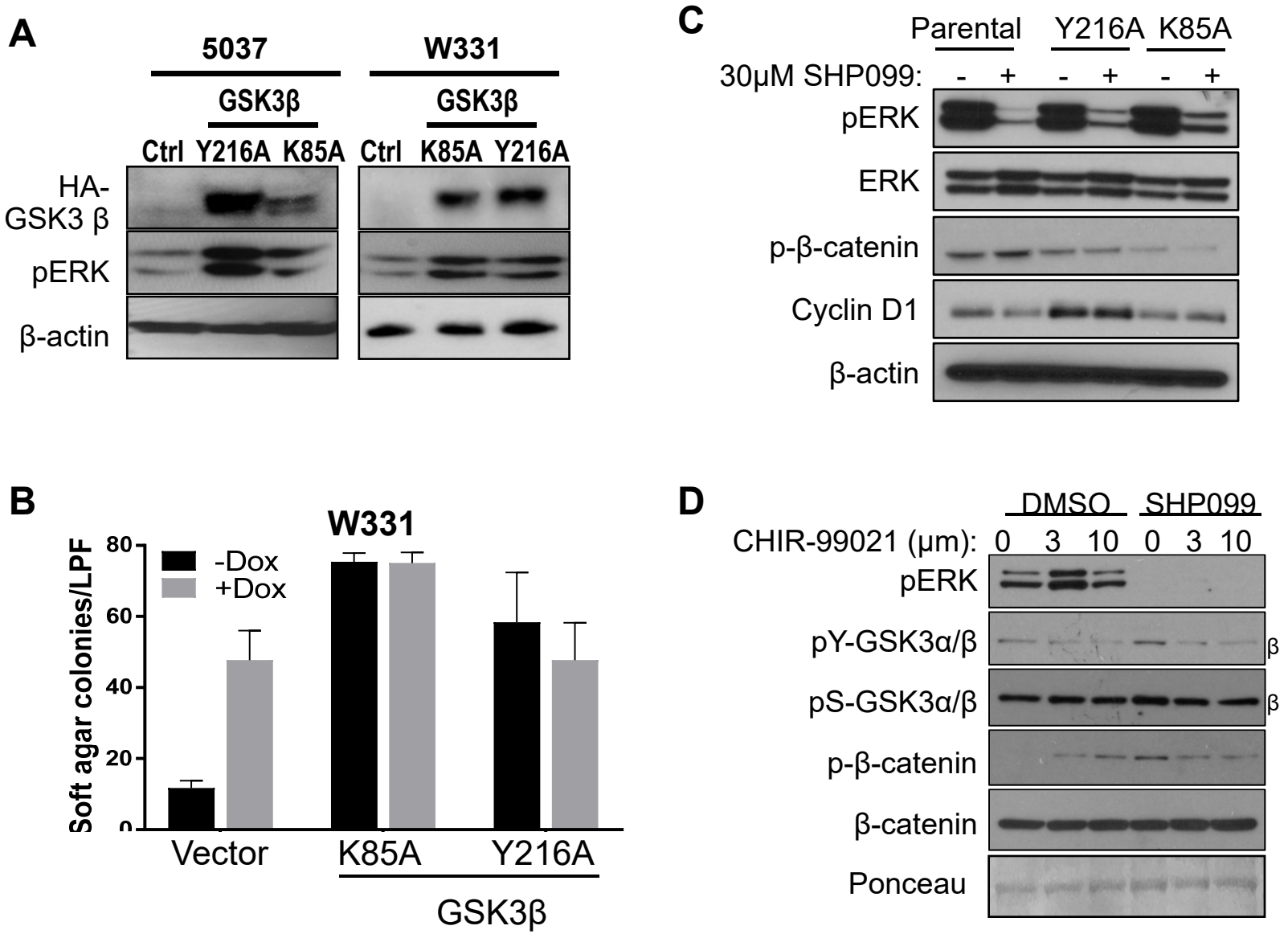

Supplementary Fig. S11

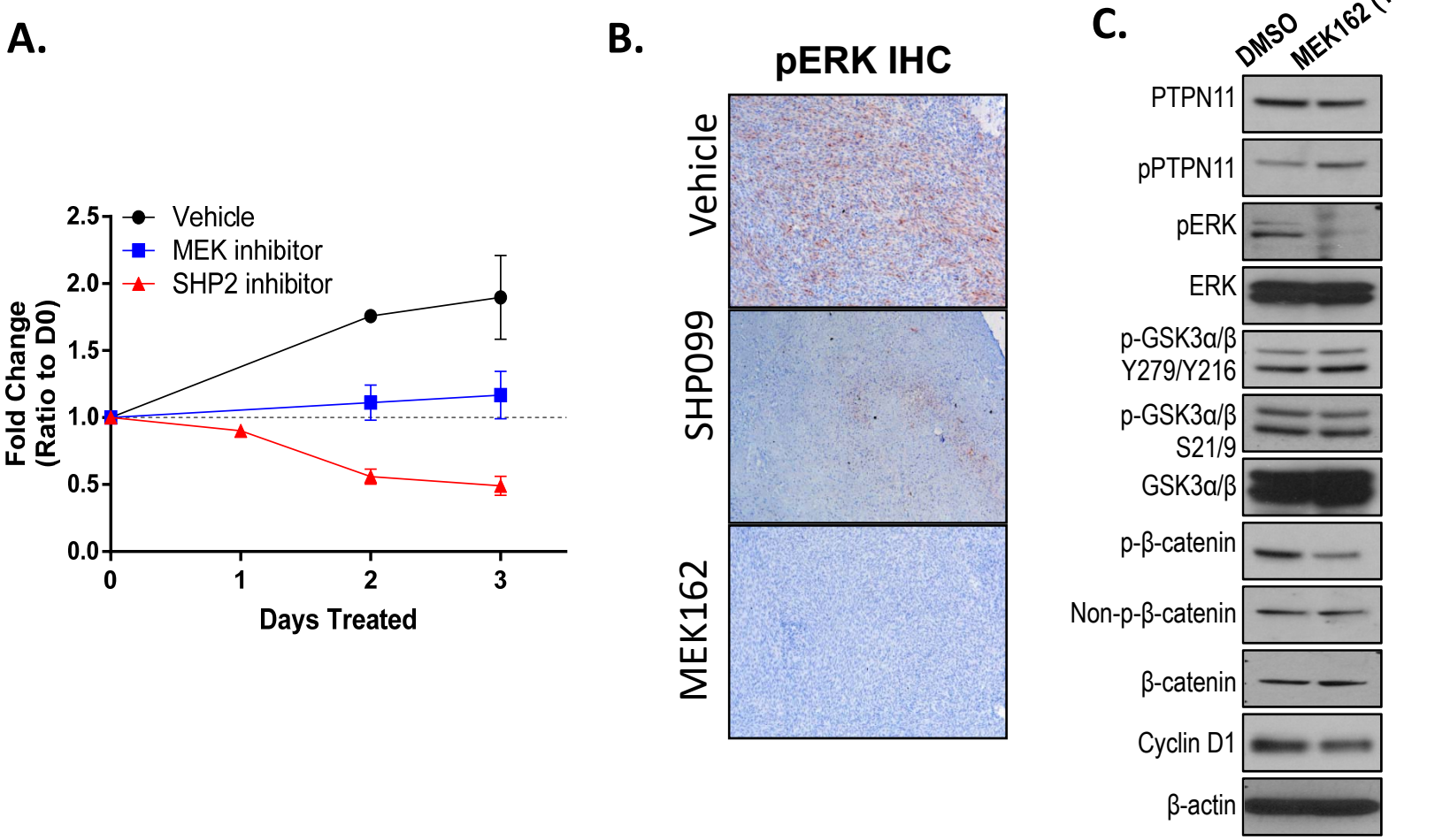

Supplementary Fig. S12

A.

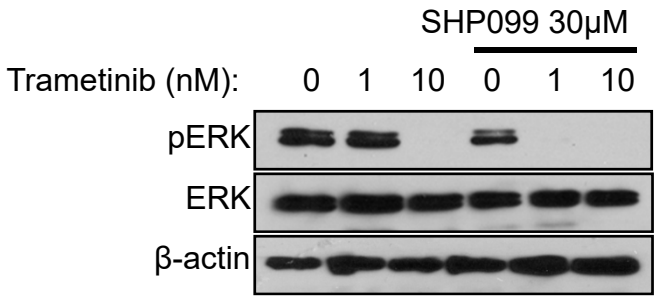

B.

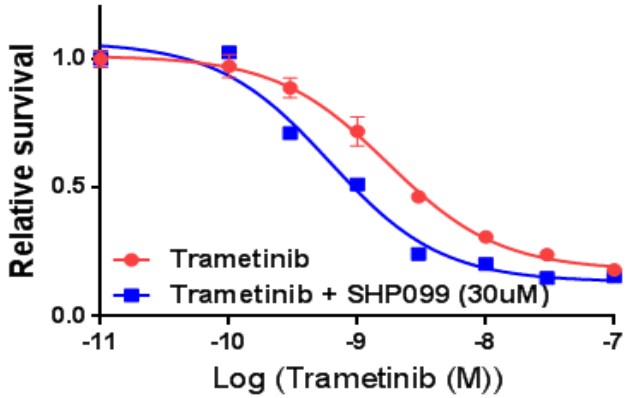

C.

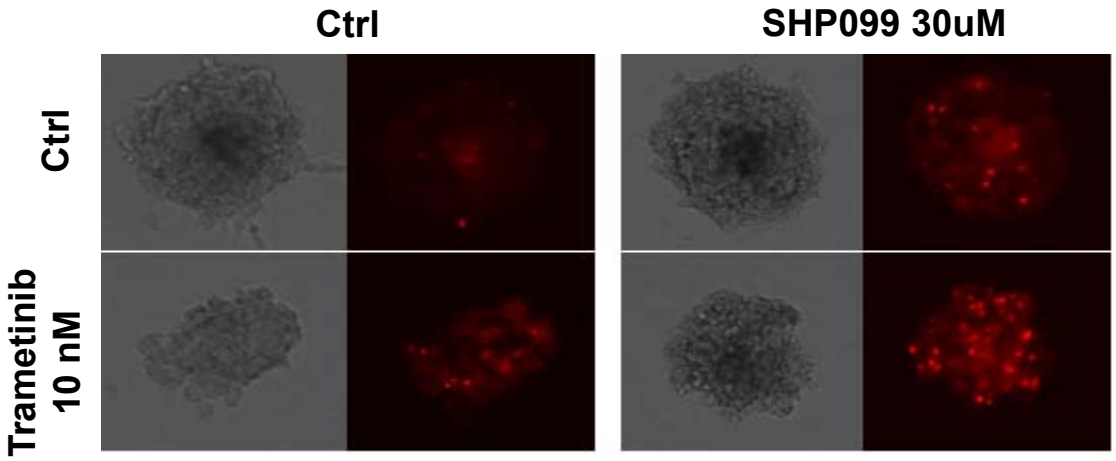

WM1366

Supplementary Fig. S13

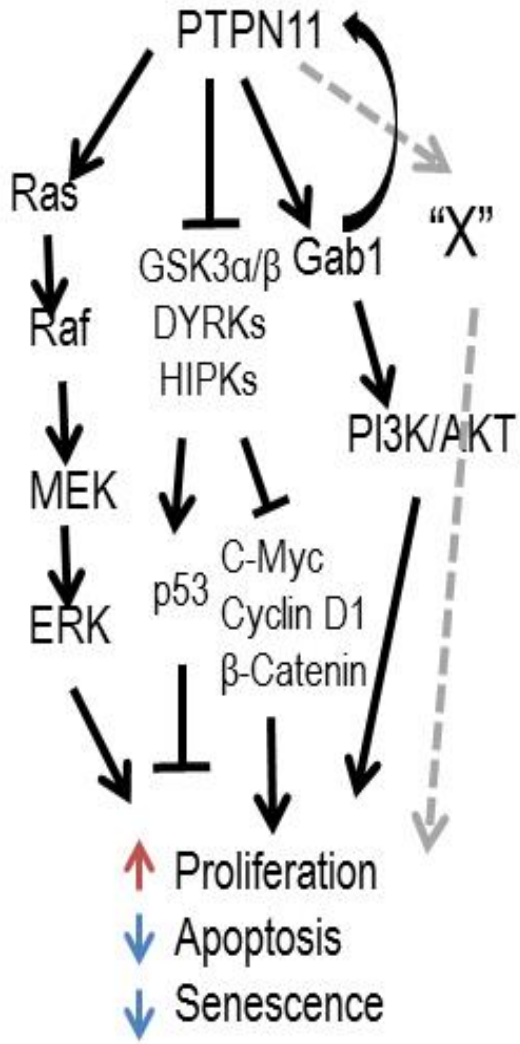

Supplementary Fig. S14